JOURNAL OF MATERIALS SCIENCE 29 (1994) 1388–1393

Structural studies on an ORMOCER system containing zirconium

A. HELMERICH*, F. RAETHER
Fraunhofer-Institut für Silicatforschung, W-8700 Würzburg, Neunerplatz 2, FRG
D. PETER, H. BERTAGNOLLI
Institut für Physikalische Chemie, W-8700 Würzburg, Marcusstrasse 9/11, FRG

The modified precursor $Zr(^{n}OPr)_3OOMc$ (McOOH = methacrylic acid) has been successfully used to synthesize organically modified ceramics (ORMOCERs) via a sol–gel process and via ultraviolet (u.v.) curing. The precursor and the ORMOCERs were investigated by the measurement of X-ray absorption fine structure (XAFS) and by electron microscopy. A model for the structure of the precursor is proposed. In the case of the inorganic synthesis of the ORMOCER, a first indication of a bond of the type Zr–O–Si was found.

1. Introduction

New quality standards in materials science can be set by combining organic and inorganic materials on a molecular level. To avoid high temperatures in the manufacture of these hybrid materials, a sol–gel process was envisioned as a possible route [1]. Partially hydrolysing alcoholic solutions of metal alkoxides leads to a sol which eventually condenses to a gel. The resulting material (ORMOCER, organically modified ceramic [2]) proved to have a rich potential for future applications. Indeed it was found that while the sol–gel process was an inorganic route of forming an inorganic–organic material organic links could also be sought via unsaturated organic ligands attached to the metal alkoxides. Therefore a model system was chosen (Fig. 1) which enabled both of the above approaches to be studied. This model system also has practical importance as it forms the base system for a scratch-resistant varnish [3]. With some alterations it can also be applied to protect historic stained-glass windows [4].

To picture the structural differences using the inorganic route via the sol–gel process or the organic route via u.v.-irradiation, scanning transmission electron microscopy (STEM) and X-ray absorption spectroscopy (XAFS) were chosen as methods of probing the samples.

One of the earliest theories about the structure of metal alkoxides was advanced in 1958 by Bradley [5]. He predicted a trimeric structure for all zirconium tetra-alkoxides. This was confirmed for $Zr(^{i}OPr)_4$ in benzene, whereas in $^{i}PrOH$ Bradley found dimers to be the smallest units. The latter was explained by the formation of a complex between the alkoxide and the solvent: $Zr(^{i}OPr)_4{}^{i}PrOH$ [6]. An interesting question to answer is how the formation of the complex and the subsequent reaction with the silicon compound alters the zirconium compound.

2. Experimental section

2.1. Samples

Referring to Fig. 1, zirconium *n*-propoxide (Zp), purchased from Hüls AG as a 2.2 M solution of $Zr(^{n}OPr)_4$ in *n*-PrOH, was reacted with methacrylic acid (McOOH) in a molar ratio. Care was taken that the temperature during the forming of the complex, did not rise by more than 10 degrees. McOOH allowed the controlled hydrolysis of the metal alkoxide and u.v. curing of the system at the same time. Because it was not possible to react vinyltriethoxisilane (VTEOS) with Zp via the sol–gel route or to use vinyltrimethoxisilane (VTMOS) for u.v. curing, the system had to be slightly modified for the two routes (Fig. 1).

In the first case, the Si-component (VTMOS) was partially hydrolysed by adding water and the catalyst, methylimidazol (MI), in a molar ratio of 1 : 1.5 : 0.1 and stirred until the mixture became clear, then it was added to the complexated Zp. The sol started to gel and resulted in a transparent monolith within two days. Without losing transparency, the molar ratio of Zr : Si could be varied from 0 : 1 upto 1 : 1. For this study, an ORMOCER with the composition Zr : Si = 2 : 5 is shown.

Following the organic route, the Si-compound (VTEOS) was added together with a radical initiator (IRGACURE 184) to an equivalent of the complexated Zp. The mixture was then applied to a glass slide and irradiated under nitrogen by two u.v. light bulbs (LOCTITE UVA 1000) to avoid the entry of moisture.

2.2. XAFS

X-ray absorption measurement at the Zr–K edge was performed on beam-line RöM01 using synchrotron radiation delivered by DESY (Hamburg). The energy of the electrons in the beam was 5.3 GeV and the

* *Present Address*: Siemens/Nixdorf AP82 MchP/Pb, Otto-Hahn-Ring 6, W-8000 München 83, FRG.

0022–2461

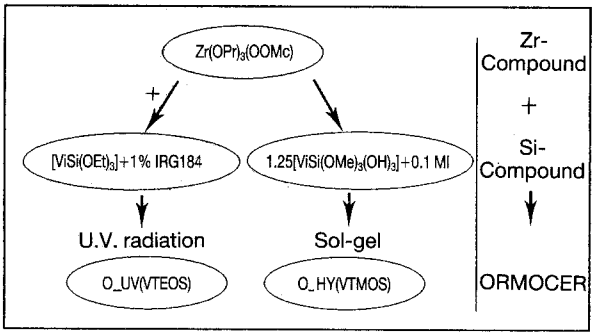

Figure 1 Schematic description of the inorganic (sol–gel) and organic (u.v. curing) modes of synthesizing mixed organic–inorganic hybrid materials (ORMOCERs). (McOOH = methacrylic acid, VTEOS = vinyltriethoxisilane, VTMOS = vinyltrimethoxisilane, IRG 184 = IRGACURE 184, and MI = methylimidazol).

stored current varied from 50 to 20 mA. The X-ray beam was monochromated by a (3 1 1) Si double-crystal monochromator and detected with ionization chambers filled with nitrogen gas.

The solutions were kept in steel cells containing two Kapton windows, which were sealed against moisture (Kapton 120 F 612, 25 μ, DuPont Electronics). The thickness of the cell was adjusted to cause a jump of $\mu x \approx 1.5$ at the Zr–K edge in the XAFS spectra. The solid samples were grained under nitrogen and filled into a steel block also sealed with Kapton windows. The absorption was, in this case, adjusted by mixing the substances with boro nitride.

The energy interval of 17.85–18.90 keV was scanned in such a way as to give an average resolution in k-space of 0.5 nm^{-1}. For each run ($\approx$ 12 min) the energy was rescaled taking the maximum of the first derivative for the edge (17.998 keV). The spectra were deconvoluted using a Gaussian monochromator resolution function with a half-width of 7.5 eV and the algorithm of Sauder [7]. The width was estimated by measuring the width of the edge. Following the standard procedure [8], the pre-edge was subtracted using an apt victoreen function. The continuous absorption background, μ_0, was calculated using a smoothing spline technique [9]. Without weighting the data points, good results were obtained with a smoothing factor, SM, of 50 %. A smoothing factor of 100 % was defined by fitting a straight line. At this stage several runs were averaged to improve the signal-to-noise ratio. Estimating the experimental error on the basis of shot noise only results in a ratio of better than 10 000 : 1 for the raw data.

The near-edge fine structure (NEXFS) was simply plotted and compared, since no exact theory currently exists. From the normalized and k^3-weighted fine structure (EXAFS extended X-ray), structural information was extracted using the computer program EXCURV'90 [10] with rapid curved-wave theory [11]. The mean free path of scattered electrons was calculated from the imaginary part of the potential (VPI = -4 eV), the amplitude-reduction factor was fixed at 0.8 and an overall energy shift was introduced to best fit the data (ΔE_0 = 24–26 eV).

2.3. STEM

Supplementing a conventional scanning transmission electron microscope (Philips, CM 12) with a cryogenic sample holder (Gatan, type 626) allowed frozen liquids (-160 °C) to be viewed in the vacuum of the electron microscope. To prepare the samples, a closed-environmental cell was constructed following the ideas of Bailey *et al.* [12]. Inside it, a copper grid coated with a holey carbon film (Plano, S-166) was inserted into the liquid sample and then blotted, to leave only a very thin film of the sample on the grid ($\approx$ 100 nm). The grid was then plunged into liquid propane which was cooled by liquid nitrogen.

Using an energy dispersive spectroscopy (EDX) detector (EDAX, PV 9800) in addition, the chemical composition of the sample was analysed. Subtracting the background and relating the peak area of the Zr-Kα line to the area of the SiKα line at various spots (ϕ = 7.5 nm) along a line through a particle resulted in a line scan of the elemental distribution of that particle ($\phi \approx$ 300 nm).

3. Results and discussion

3.1. Zirconium *n*-propoxide (Zp)

Fig. 2a gives an experimental EXAFS spectra $k^3[\chi(k)]$ of Zp. The Fourier transform of the signal shows the phase-corrected radial distribution function (Fig. 2b). Using a minimum of six shells, the EXAFS spectra can be simulated by a dimeric model (Fig. 4). With less shells, there was no success in reproducing the EXAFS spectra and the radial-distribution function simultan-

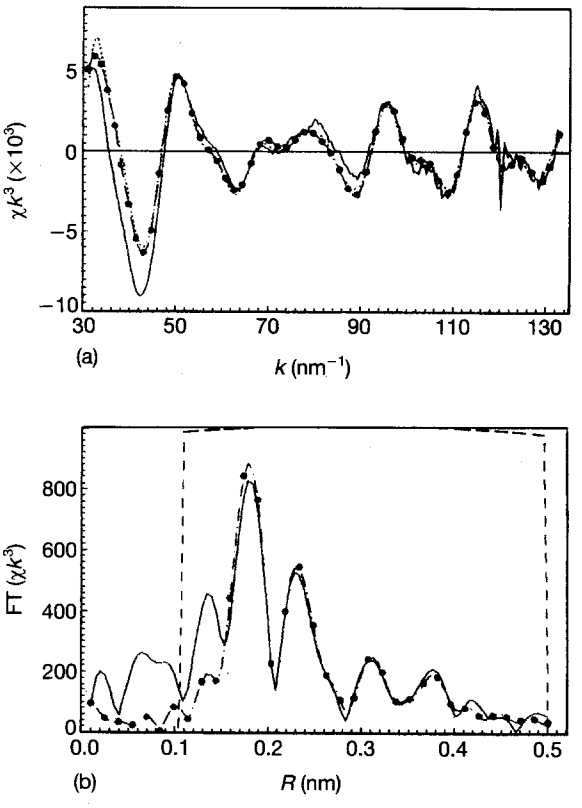

Figure 2 (a) (—) Normalized EXAFS spectrograph, $k^3[\chi(k)]$, versus k (nm^{-1}), of a solution of Zr (^{n}OPr)$_4$ in *n*-HOPr compared with (●) a theoretical model using six shells, and (...) the filtered experimental EXAFS results. The latter were generated using a Gaussian window: $\exp\{-0.5[(R-0.3)10]^2\ nm^{-2}\}$ in R-space. (b) Phase-corrected Fourier transform (FT) of (a) and the Gaussian window: (—) experimental, (●) six shells, (—·—) Gaussian curves.

eously. The discrepancies between the experimental and theoretical spectra in the range 30–50 nm^{-1} and 70–90 nm^{-1} may be attributed to the atomic EXAFS. The latter is responsible for the signal at low R-values (< 0.15 nm) in the radial-distribution function. These signals can only be separated by Fourier filtering (with a Gaussian window from 0.1 to 0.5 nm). The back-transformed EXAFS function is in excellent agreement with the theoretical-model function.

By normalizing and weighting the EXAFS spectra, the signal-to-noise ratio for high k-values is much less favourable. In Fig. 3a the effect of the outer shells is compared to the noise level. A subdivision of the outer shells into two carbon and one zirconium shell is not advisable since the various contributions partially cancel each other. This can clearly be seen in R-space if the zirconium shell is omitted in the model function while the other shells are left unchanged (Fig. 3b).

The fitting results are given in Table I. The findings can be fully explained if it is assumed that the oxygen of the alkoxide bridge is positioned asymmetrically between the two zirconium atoms (cf. Fig. 5). Though only a dimeric model is needed it cannot be distinguished from a trimer because the co-ordination numbers are rather vague. Firstly, they cannot be taken as absolute numbers because of the uncertainty in the amplitude–reduction factor. Secondly, they are too strongly correlated with the Debye–Waller factors and the number of shells to be treated separately.

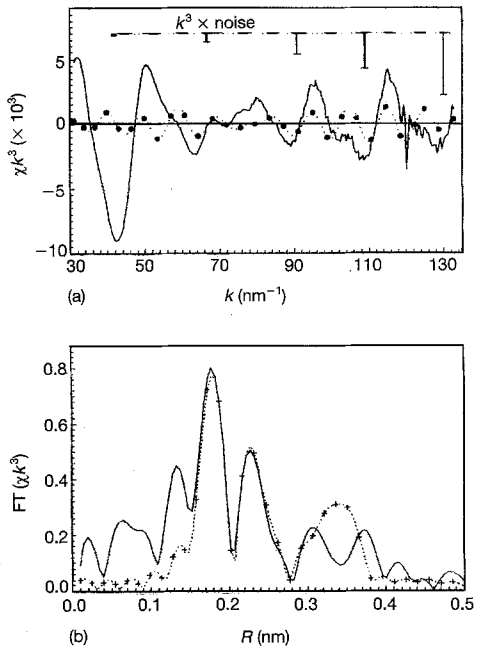

Figure 3(a) (—) Normalized-EXAFS $k^3\chi(k)$ versus k (nm^{-1}) of a solution of Zr("OPr)$_4$ in n-HOPr (as in Fig. 2a) compared with (●) a model function (diff), of the three outer shells only (two carbons, one zirconium), (—···—) an estimated weighted noise. (b) Fourier transform of (—) the experimental EXAFS in (a) compared with (+) a model function in which the zirconium shell has been omitted, to show the effect of interference.

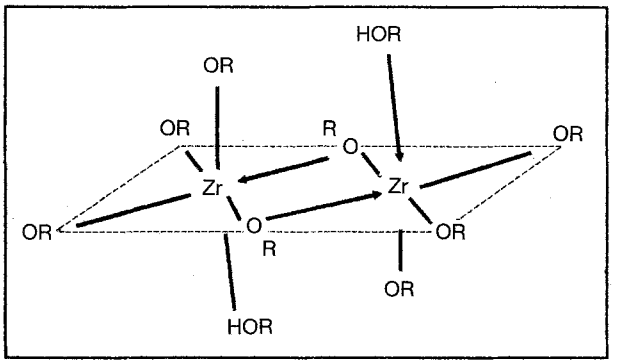

Figure 4 Dimeric model for Zr("OPr)$_4$·n-PrOH based on a similar model by Vaarstra *et al.* [6]. For the differences between these two models refer to Fig. 5.

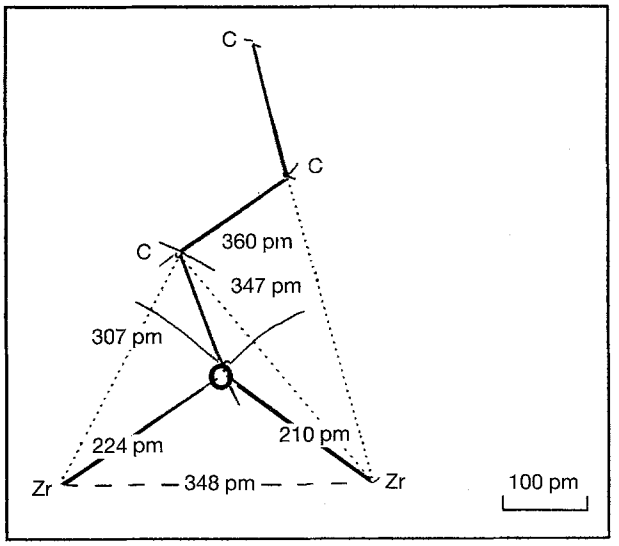

Figure 5 Construction of the geometry of the bridging alkoxide in Zp, based on the distances as they were obtained from EXAFS measurements.

TABLE I EXAFS fit parameters for zirconium n-propylate (cf. Fig. 2) found using the computer program EXCURV'90. The errors were estimated by comparing the fit parameter for different starting points. For clarity, the back scatterers in the various shells are assigned to the ligand they belong to.

Back scatterer	Distance R(pm)	Co-ordination number N	Debye–Waller amplitude σ (pm)	Assignment in Zp-model
O	194 ± 1	2.8 ± 0.6	4 ± 2	Terminal OPr
	210 ± 2	2.9 ± 0.8	5 ± 2	Axial/bridging OPr
	224 ± 2	3.2 ± 0.4	9 ± 3	Bridging/co-ordinated OPr
C	307 ± 2	1.9 ± 0.4	10 ± 5	Bridging OPr
	347 ± 4	3.7 ± 0.9	2 ± 5	Bridging OPr
Zr	348 ± 3	1.0 ± 0.4	6 ± 3	Bridging ZrOZr

Fig. 6 (a) An image of a 0.6 M solution of $Zr(^nOPr)_4$ in *n*-PrOH taken with an electron microscope at − 178° C. An analysis of the size of the particles in Fig. 6a gives the distribution in Fig. 6b, with the smallest particles having a diameter of about 1 nm. Since the phase contrast results from a fluctuation in the electron density the locations of the zirconium atoms are mostly seen and thus there is a tendency to underestimate the size of the particles. We therefore propose the smallest units to be dimers or trimers.

3.2. Complexation of zirconium *n*-propoxide with methacrylic acid

Although zirconium tetra-acetate was investigated as early as 1972 [13], it was not realized until 1987 [14] that organic acids might modify the stability towards hydrolysis of the metal-alkoxide precursors.

$$Zr(OR)_4 + McOOH \rightleftarrows Zr(OR)_3(OOMc) + ROH \quad (1)$$

Generally there are three possible types of complex: a monodental, a bidental and a chelating complex. According to an infrared measurement, the first type can be excluded [15].

The EXAFS signal $k^3[\chi(k)]$ and the phase-corrected Fourier transform of a solution of complexated Zp are shown in Fig. 7. In simulating the signal, a new carbon shell had to be introduced, which can only be understood if the McOOH is assumed to act as a chelating ligand.

Potentiometric titration of the complexation of Zp with McOOH at ambient temperature resulted in saturation at an uptake of about 1.8 equivalent of McOOH [15]. Following the reaction with a vapour-pressure osmometer, a steep increase in temperature was detected at about the same molar ratio. With infrared, the rise in temperature can be correlated with the presence of free McOOH. Observations over a period of some weeks showed that the free acid reacts with the solvent, liberating water by esterification and initializing the growth of crystals. Isolating the reaction compounds, it was found that only a maximum of 2 mol McOOH per mole Zp can be co-ordinated [15].

One could explain this limit by assuming that each McOOH increases the co-ordination number of oxygen around zirconium by one. Such a change in the

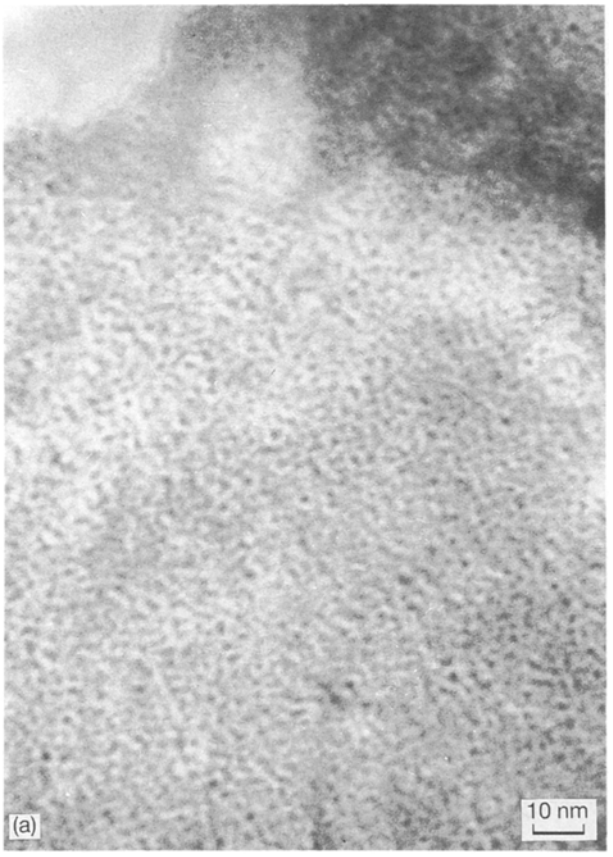

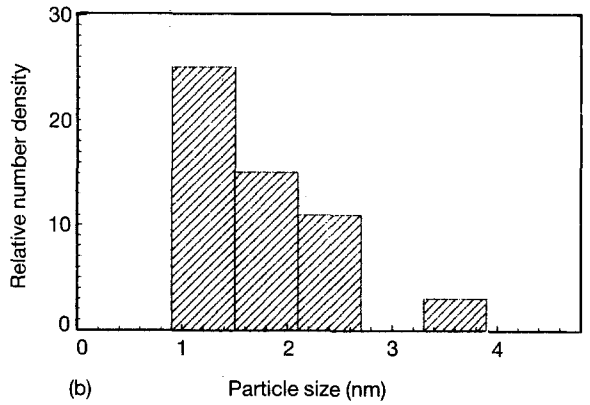

Figure 6 (a) Cryogenic TEM image of a 0.6 M solution of $Zr(^nOPr)_4$ in *n*-PrOH at − 178 °C. The dark particles are oligomeric zirconium-propoxide molecules. (b) Particle-size distribution in a frozen solution of $Zr(^nOPr)_4$ in *n*-PrOH. The contrast arises from inhomogeneities in the electron distribution function.

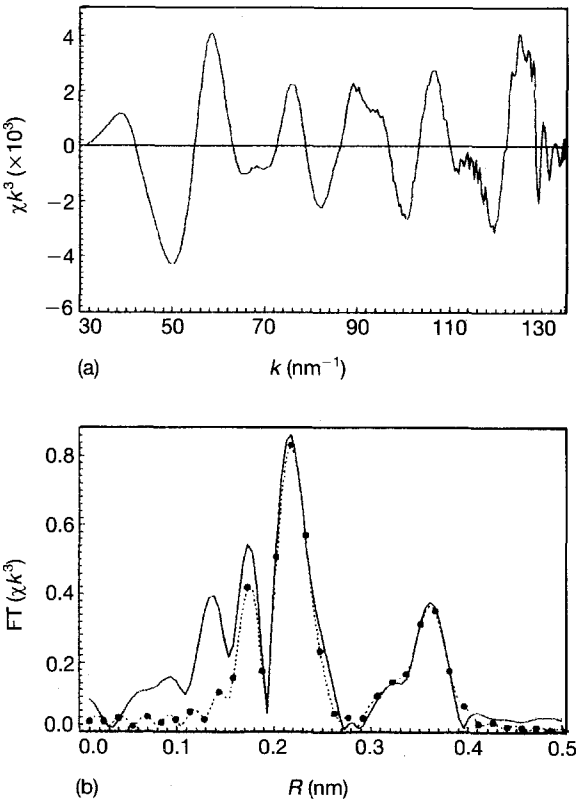

Figure 7 (a) Normalized-EXAFS k^3 $\chi(k)$ versus k (nm^{-1}) of a solution of complexated Zp and a model function: (—) experimental, and (●) six-shells model. (b) Phase-corrected Fourier transform of (a): (—) experimental, and (●) theoretical results.

TABLE II EXAFS fit parameters for complexated zirconium *n*-propylate (cf. Fig. 7) found with EXCURV'90. The errors were estimated by comparing the fit parameter for different starting points. For clarity, the back scatterers in the various shells are assigned to the ligand they belong to.

Back scatterer	Distance R(pm)	Co-ordination number N	Debye–Waller amplitude σ (pm)	Tentative assignment
O	191 ± 2	1.7 ± 0.6	2 ± 2	Terminal OPr
	208 ± 4	3.1 ± 0.8	4 ± 2	Axial/bridging OPr/OOMc
	221 ± 4	3.6 ± 0.6	4 ± 3	Bridging/co-ordinated OPr/OOMc
C	238 ± 3	1.3 ± 0.5	5 ± 5	Chelating OOMc
	314 ± 4	0.9 ± 0.8	7 ± 5	Bridging OPr
	348 ± 2	5.1 ± 1.1	8 ± 5	Bridging OPr
Zr	345 ± 3	1.0 ± 0.4	5 ± 3	Bridging ZrOZr

co-ordination number would also explain the observed changes in the near-edge (NEXFS) region.

3.3. ORMOCERs containing zirconium

If a reaction is postulated for the inorganic route leading to a bond of the type Zr–O–Si a Zr–Si correlation in 365–375 pm would be expected according to the angle of the bridge. Since the probing was from the Zr side, an excess of the Si compound should increase the probability of finding the correlation. If on the other hand a linking is postulated of the $McOO^-$ ligand with the vinyl group of VTEOS during u.v. curing, no Zr–Si correlation is expected before $R = 550$ pm. In Fig. 8 the radial-distribution functions of the ORMOCERs prepared by an inorganic sol–gel route and by an organic u.v.-curing process are compared. Since the first reaction is started by hydrolysing VTMOS, the resulting ORMOCER is denoted by QHY(VTMOS) whereas the latter ORMOCER is called QUV (VTEOS).

Simulating the spectra and comparing them to the spectra of complexated Zp it is found that, in both cases, the first six shells were hardly affected by the reaction with the silicon component. However, including a seventh shell with Si at a distance of 377 pm then, in the case of QHY(VTMOS), the fit index (FI) can be slightly improved from 3.57 to 3.55

$$\mathrm{FI} = \frac{1}{100N} \sum_{i=1}^{N} [(\chi_i^{\exp} - \chi_i^{\mathrm{fit}})\, k^3]^2$$

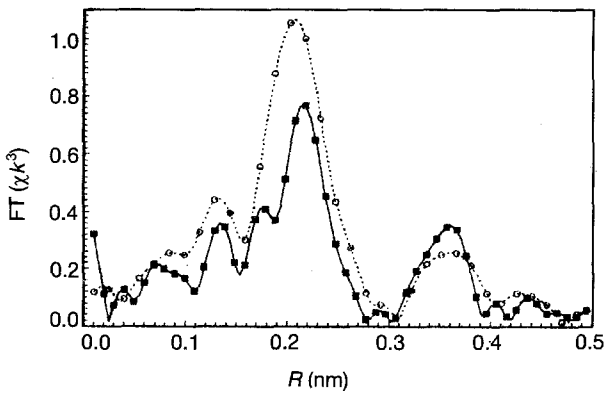

Figure 8 Comparison of radial-distribution functions of ORMOCERs prepared: (○) by an inorganic sol–gel route (QHY(VTMOS)), and (■) by an organic u.v.-curing process (QUV(VTEOS)).

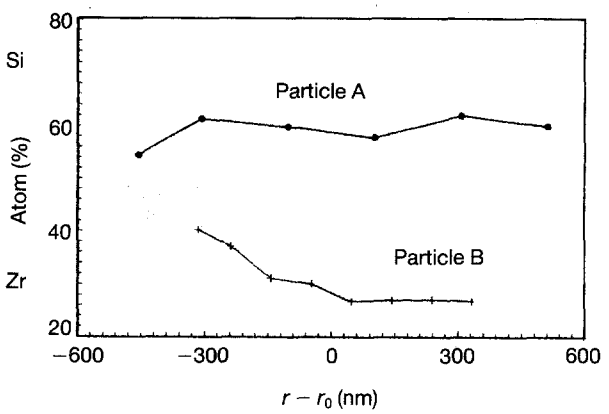

Figure 9 Line scan of two grains of the ORMOCER QUV(VTEOS) using the ratio of the ZrK_α and the SiK_α absorption-peak area of an EDX detector.

(cf. [10]). A similar improvement was not observed in the case of the QUV(VTEOS). This could be taken as a first indication of a bonding of the type Zr–O–Si. Both types of ORMOCERs were ground and analysed with the EDX detector of the STEM. Analysing a line scan (Fig. 9) with an estimated experimental error of about 10 %, the composition of each particle was found to be more or less uniform. However, the composition showed large fluctuations from particle to particle. These observations were made on both types of ORMOCERs.

4. Conclusion

Inorganic–organic hybrid materials (ORMOCERs) can be synthesized by an inorganic sol–gel process or by an organic u.v.-curing process. The microstructure is influenced by the structure of the precursors and by the synthesis route.

Zirconium *n*-propoxide (Zp) was found to consist of dimers or trimers which were formed by bridging alkoxide ligands. In complexating Zp with methacrylic acid, a terminal alkoxide group was exchanged by the methacrylic ligand, which formed a chelate complex within the aggregate.

Using hydrolysis and condensation to form an ORMOCER, a first indication was found of a bond of the type Zr–O–Si. Although on a scale of a few hundred nanometres the ORMOCER has a rather uniform composition, there are huge differences on a grain-to-grain scale.

References

1. R. ROY, *J. Amer. Ceram. Soc.* **39** (1956) 146.
2. H. SCHOLZE, *J. Non-Cryst. Solids* **73** (1985) 669. H. Schmidt, in "ACS symposium series" (American Chemistry Society, Washington, 1988) p. 333.
3. S. AMBERG-SCHWAB, E. ARPAC, W. GLAUBITT, K. ROSE, G. SCHOTTNER and U. SCHUBERT, in "High performance films and coatings" edited by P. Vincenzini (Elsevier Science, Amsterdam, 1991) p. 203.
4. H. RÖMICH and D. R. FUCHS, in "FhG-tätigkeitsbericht 1989" (Fraunhofer-Institut für Silicatforschung, Würzburg, 1990) p. 40.
5. D. C. BRADLEY, *Nature* **182** (1958) 1211.
6. B. A. VAARSTRA, J. C. HUFFMAN, P. S. GRADEFF, L. G. HUBERT-PFALZGRAF, J.-C. DARAN, J. PARRAND, K. YUNLU and K. G. CAULTON, *Inorg. Chem.* **29** (1990) 3126.
7. W. C. SAUDER, *J. Appl. Phys.* **37** (1966) 1493.
8. B. K. TEO, "EXAFS: basic principles and data analysis", (Springer Verlag, Berlin, 1986).
9. C. H. REINSCH, *Numer. Math* **10** (1967) 177.
10. N. BINSTED, J. W. CAMPBELL, S. J. GURMAN and P. C. STEVENSON, SERC Daresbury Laboratory EXCURV'90 Computer Program (Science and Engineering Research Council, Daresbury, England, 1990).
11. S. J. GURMAN and N. BINSTED and I. ROSS, *J. Phys. C* **17** (1984) 143.
12. J. K. BAILEY, J. BELLARE and M. L. McCARTNEY *Mater. Res. Soc. Symp. Proc.* **115** (1988) 69.
13. V. L. PAVLOV, YU. A. LYSENKO and A. A. KALINICHENKO, *Russ. J. Inorg. Chem.* **17** (1972) 1768.
14. S. DEUFF, M. HENRY, C. SANCHEZ and J. LIVAGE, *J. Non-Cryst. Solids* **89** (1987) 206.
15. U. SCHUBERT, E. ARPAC, W. GLAUBITT, A. HELMERICH and C. CHAU, *Chem. Mater.* **4** (1992) 291.

Received 15 May 1992
and accepted 16 April 1993